Hindawi
Advances in Civil Engineering
Volume 2019, Article ID 5171873, 11 pages
https://doi.org/10.1155/2019/5171873

Research Article

Influence Law of Interbedded Strata and Their Collapse on the Mining of Extremely Thick Coal Seam under Goaf

Chunxu Ji,[1] Yongkang Yang,[1,2,3,4,5] Xingyun Guo,[5] Tianhe Kang,[1] and Zefeng Guo[1]

[1]*Key Laboratory of In-Situ Property-Improving Mining of Ministry of Education, Taiyuan University of Technology, Taiyuan, Shanxi 030024, China*
[2]*State Key Laboratory for Geomechanics & Deep Underground Engineering, China University of Mining & Technology, Xuzhou 221116, Jiangsu, China*
[3]*State Key Laboratory of Coal Resources and Safe Mining, China University of Mining & Technology (Beijing), 100083 Beijing, China*
[4]*Research Center of Coal Resources Safe Mining and Clean Utilization, Liaoning Technical University, Fuxin Liaoning 123000, China*
[5]*Department of Mining Engineering and Metallurgical Engineering, Western Australian School of Mines, Curtin University, Kalgoorlie 6430, Australia*

Correspondence should be addressed to Yongkang Yang; yongkang8396@163.com

Received 8 August 2018; Accepted 10 January 2019; Published 11 February 2019

Guest Editor: Guo-zhong Hu

Interbedded strata and their collapse are vital to mining pressure control for extremely thick coal seam under goaf. To ensure the stability of the support and to avoid roof collapse, some traditional underground pressure theoretical models had been widely used in the control of surrounding rock and the selection of support. However, one of the challenges for extremely thick coal seam under goaf is that the abnormal disasters, such as support crushing and water inrush that were occurring frequently. To solve this problem, the movement characteristics of overburden rocks during the mining of extremely thick coal seam under the conditions of the interlayer thickness of 5 m and 40 m were studied by using the similar simulation experiments, while the numerical simulation experiments were carried out for the interval between coal seams of 15 m and 60 m, respectively. Finally, the structure and mechanical transfer mechanism of overburden in stope under different thickness interbedded strata were analyzed dynamically, and the condition of full-thickness connection between upper goaf and lower goaf and corresponding judgment criteria are obtained. These results can guide future research on the mechanical of extremely thick coal seam under goaf, which can provide a theoretical basis and engineering reference for similar projects.

1. Introduction

With the depletion of shallow coal resources, coal mining operations were gradually transferred to a single extremely thick coal seam with a thickness of 6–25 m [1, 2]. In China, there exist a great number of the coal seams with the abovementioned conditions in Shanxi, Shaanxi, Inner Mongolia, Xinjiang, and other regions. Therefore, a feasible mining method is significant for these coal seams [3, 4]. This study was conducted in Xiegou Coal Mine (No. 13 coal seam under No. 8 goaf). The first working face (23103) is exposed to abnormal disasters such as support crushing and water inrush, which also indicates it is not viable to deal with the extremely thick coal seam simply based on the theory of traditional mine pressure.

The redistribution of surrounding rock stress induced by coal mining operations, the intensive stress, and stress transfer to the deeper extensively exist when mining operations are developed deeper. Meanwhile, these problems bring difficulties in the mining operations [5–7]. Close-distance coal seams refer to coal seams with small coal seam spacing and substantial influence on each other at mining operations [8–11]. As a result, the upper coal seam mining damages the surrounding rock and then transmits stress to the bottom

plate [10–13]. Yan [14–17] conducted a preliminary study on the joint mining theory of short-distance thin coal seams; Zhu et al. [18] conducted a relevant theoretical investigation with the following assumption: the interlayer and upper degraded rock formation were regarded as a block and a loose body, respectively. Due to the variation of coal seam occurrence conditions and interlayer distance, the mine pressure performance of the fully mechanized coal mining face has various characteristics [19–24]. Under this condition, it is difficult to determine the load of working faces simply based on the traditional theory of roof support and control.

In addition, several problems (e.g. water, fire, gas, and mine pressure disasters) in extremely thick coal seams become increasingly serious. The spacing between the coal seam and upper goaf ranges from 30 to 80 m. For ordinary working faces, there will be no obvious safety problems for downward mining, but for the 15 m thick coal seam, the fault zone will directly penetrate the upper goaf. The fractured rock mass transmits the load, and the main roof breaking movement may directly affect the surface; in the presence of the coal pillar in the upper goaf, there may be harmful gas accumulation and wastewater enrichment, which may cause accumulation of gas in the mining of the underlying thick coal seam and even coal seam spontaneous combustion, water inrush, and other disasters [3,24–28]; residual coal pillars in the goaf to transfer stress concentration may suddenly lose stability or cause impact pressure [7, 29]. The actual measurement of the mine pressure in the Xiegou coal mine, the Tashan coal mine, and the Suancigou coal mine shows that, under goaf (especially under the coal pillar), the lower working resistance of the hydraulic supports is common for the fully mechanized caving mining in the extremely thick coal seam but occasionally shows abnormal pressures such as support crushing and water inrush. Therefore, whether it continues to improve the working resistance of the hydraulic supports is a topic worth considering. Therefore, whether the stope continues to improve the working resistance of the bracket is a topic worth considering.

The overlying strata structure of the mining of extremely thick coal seam under goaf will form a structure similar to the shallow buried depth rather than the shallow buried depth, and the structure is similar to the thick alluvium while not the thick alluvium. Mostly, the pedestal rock of the shallow coal seams is thinner, and the surface is loosely covered. The mining pressure of the shallow working face is severe, and the loose covering layer moves with the bedrock layer and falls on the surface, which is prone to abnormal disasters and water or sand inrush. Huang and Xu have conducted relevant studies of this aspect [30–33]; as the thick alluvium is extensively excavated in the bottom coal seam, the alluvium is integral in the motion deformation, its self-weight will be acting on the underlying bedrock in the form of loads, while the bearing capacity of the bedrock is easily analysed and the roof of the working face can be controlled easily [34–36]. The overlying strata structure of the mining face with large mining height and fully mechanized caving mining under the goaf has its own particularity, and the overlying goaf generally contains wastewater from the upper goaf, which is prone to water inrush from the roof. The relationship between the surrounding rock and the support is still unclear, especially the mechanism of the support crushing is not enough. Under the background of a large amount of extremely thick coal resources buried in the goaf in China, relevant research needs to be carried out.

2. Physical Simulation Test on Different Thickness of Interbedded Strata and Their Collapse

2.1. Prototype Geological Conditions. Shanxi Coking Coal Group's Xiegou Coal Mine has a designed production capacity of 15 million tons per year. The minefield is 22 km long from north to south, 4 to 5 km wide from east to west, and covers an area of 88.64 km^2. It mainly mines Nos. 8 and 13 coal seams. The average thickness of the No. 8 coal seam is 5.7 m, the average thickness of the No. 13 coal seam is 15 m, and the spacing between two coal seams is 55 m. At present, the No. 8 coal seam in the first mining area has been completed, and the No. 13 coal seam is in the trial mining stage. The No. 13 coal seam adopts the mining method of large mining height and caving coal, with a cutting height of 4 m and caving height of 11 m.

2.2. Experimental Design. A large-scale plane strain similar simulation test platform was selected from the Institute of Mining Technology of the Taiyuan University of Technology. The effective size of the test platform is 3.0 m × 1.8 m × 0.16 m, and the geometric similarity ratio is 1 : 50. Under the conditions of model coal seam thickness 30 cm (actual 15 m) and mining height 8 cm (actual 4 m), the overburden collapse characteristics of interlayer rock thickness between 5 m and 40 m are compared and analyzed. Discrete rigid blocks were selected in similar simulation experiments.

2.3. Results and Discussion

2.3.1. Interbedded Strata Thickness of 5 m. The pressure characteristics of the working face are shown in Table 1. When the working face advances 0.46 m (23 m) close to the first coal pillar, the initial collapse of the top coal occurs (Figure 1(a)). When the working face advances 0.69 m (34.5 m), the immediate roof falls for the first time, and the fall angle is 58.22° (Figure 1(b)). When the working face is advanced by 0.56 m (28 m), the "arch structure" with the same height as the coal seam is formed. When the working face is advanced by 0.97 m (48.5 m), the main roof caves for the first time (Figure 1(c)). When the working face advances 1.1 m (55 m), 1.43 m (71.5 m), and 1.98 m (99 m), the first three periodic roof weighting occurs and the top roof collapses at the angle of 51.28°, 43.32°, and 62.80°, respectively (Figures 1(d)–1(f)). When the working face is advanced 2.23 m (111.5 m), the main roof lead fracture causes the front support point to rotate and induces deformation instability.

2.3.2. Interbedded Strata Thickness of 40 m. The working face pressure characteristics are shown in Table 2. When the working face advances 0.72 m (36 m), the top coal first falls,

Table 1: The statistics of top coal, immediate roof, and main roof collapsing interval of 10 cm (5 m) interlayer.

No.	Name	Face advanced distance		Periodic roof weighting pace	
		Model (cm)	Reality (m)	Model (cm)	Reality (m)
1	1st top coal caving	46.0	23.0	46.0	23.0
2	1st roof caving	69.0	34.5	69.0	34.5
3	1st roof weighting pace	97.0	48.5	97.0	48.5
4	1st periodic roof weighting	110.0	55.0	13.0	6.5
5	2nd periodic roof weighting	143.0	71.5	33.0	16.5
6	3rd periodic roof weighting	198.0	99.0	55.0	27.5
7	4th periodic roof weighting	231.0	115.5	33.0	16.5
8	5th periodic roof weighting	268.0	134.0	37.0	18.5
9	Average			34.2	17.1

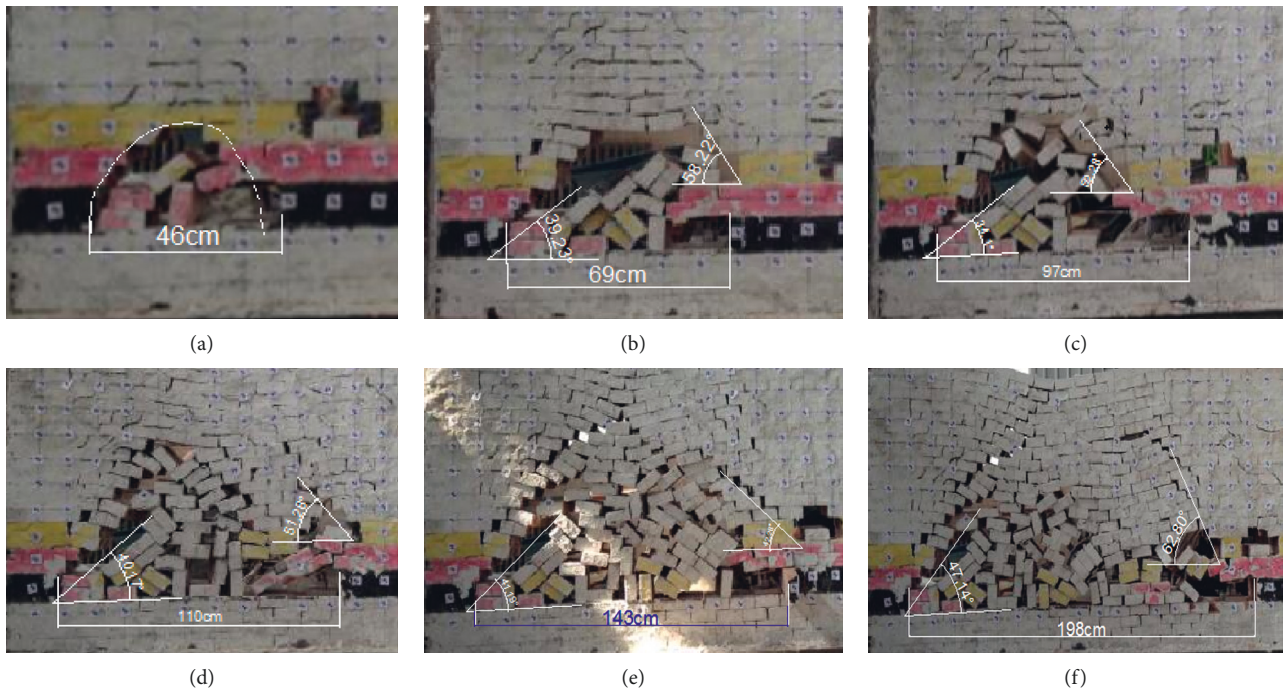

Figure 1: The advancing distance of working face and strata pressure phenomenon of stope in 10 cm (5 m) interlayer. (a) 1st top coal caving. (b) 1st roof caving. (c) 1st roof weighting pace. (d) 1st periodic roof weighting. (e) 2nd periodic roof weighting. (f) 3rd periodic roof weighting.

Table 2: The statistics of top coal, immediate roof, and main roof collapsing interval of 80 cm (40 m) interlayer.

No.	Name	Face advanced distance		Periodic roof weighting pace	
		Model (cm)	Reality (m)	Model (cm)	Reality (m)
1	Top coal caving	72.0	36.0	72.0	36.0
2	First roof caving	74.0	37.0	74.0	37.0
3	1st roof weighting pace	85.0	42.5	85.0	42.5
4	1st periodic roof weighting	122.0	61.0	37.0	18.5
5	2nd periodic roof weighting	152.0	76.0	30.0	15.0
6	3rd periodic roof weighting	185.0	92.5	33.0	16.5
7	4th periodic roof weighting	223.0	111.5	38.0	19.0
8	5th periodic roof weighting	254.0	127.0	31.0	15.5
9	6th periodic roof weighting	284.0	142.0	30.0	15.0
10	Average			33.17	16.58

and the overburden appears to be separated (Figure 2(a)). When the working face advances 0.74 m (37 m), the immediate roof falls for the first time, and the angle is 58.74° (Figure 2(b)). When the working face is advanced by 0.85 m (42.5 m), the main roof caved for the first time (Figure 2(c)). When the working face is pushed forward by 1.22 m (61 m), 1.52 m (76 m), and 1.85 m (92.5 m), the first three periodic roof weighting occurred. At this time, the top coal fell at the

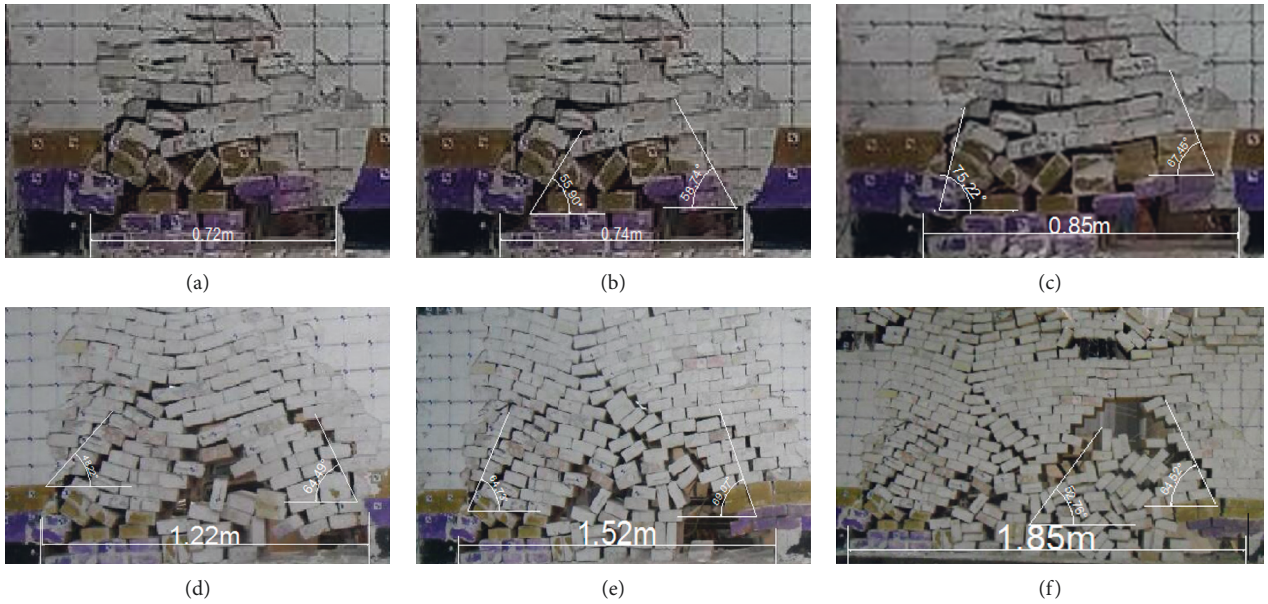

Figure 2: The advancing distance of the working face and strata pressure phenomenon of stope in 80 cm (40 m) interlayer. (a) 1st top coal caving. (b) 1st roof caving. (c) 1st roof weighting pace. (d) 1st periodic roof weighting. (e) 2nd periodic roof weighting. (f) 3rd periodic roof weighting.

fall angles of 64.49°, 69.84°, and 64.83°, respectively (Figures 2(d)–2(f)). When the work advances forward 2.12 m (106 m), the main roof lead fracture causes the front support point to rotate and will induce deformation instability.

3. Numerical Simulation Test on Different Thickness of Interbedded Strata and Their Collapse

3.1. Model Description. UDEC numerical simulation software was selected, the model width × height = 240 m × 180 m, and the upper 8th coal seam left a coal pillar with a width of 20 m (as shown in Figure 3). It is assumed that the layers of the coal and rock mass are isotropic and horizontal, the horizontal and displacement constraints are established at the bottom of the model, the horizontal constraints are established at the left and right boundaries, and the upper boundary is the stress boundary. The models of interlayer rock thicknesses of 60 m and 15 m are established. The mechanical parameters of coal-rock contact surfaces are shown in Table 3.

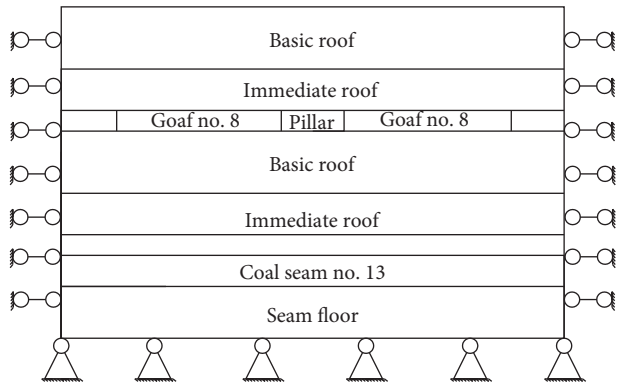

Figure 3: Initial design model.

3.2. Results of Numerical Simulation

3.2.1. Interbedded Strata Thickness of 60 m. When the working face advances 40 m, the lower immediate roof directly falls behind the working face, and the upper immediate roof is directly broken; the total damage height reaches 20 m, forming a small "arch structure" (Figure 4(a)). When the working face advances 60m, the upper immediate roof collapses, the total damage height reaches 30m, and the fracture zone is in the interbedded strata, while the small "arch structure," as have been mentioned above, expands into a larger "arch structure" (Figure 4(b)). When the working face advances 80 m, the lower main roof breaks, and the damage height reaches 40 m, and the "arch structure" does not expand significantly (Figure 4(c)). When the working face advances 100 m, it enters the coal pillar of the goaf and the lower main roof collapses, which leads to a large breakage, where the total damage height reaches 120 m and the large "arch structure" and the upper goaf are connected (Figure 4(d)). When the working face advances 140 m, it enters the goaf and the upper goaf is affected by the upper coal seam. However, the total damage height reaches the upper boundary of the model, and the bracket is in the "given deformation" state (Figure 4(e)). When the working face advances 180 m, the overburden area passes through the goaf and the bracket is in the "given load" state, with coal pillars as the axis of symmetry, forming two large "arch structures" which is shown in Figure 4(f).

3.2.2. Interbedded Strata Thickness of 15 m. When the working face is advanced 40 m, the interbedded strata collapse in the form of block structure, with a damage height up to

Table 3: The mechanical parameters of the contact surface of coal and rock.

Lithology	Normal stiffness (GPa)	Shear stiffness (GPa)	Cohesion (MPa)	Internal friction angle (°)	Strength of extension (MPa)
Pack sand	8.5	8.5	1.6	20.2	0
Medium-grained sandstone	7.0	7.0	1.5	19.5	0
Argillaceous sandstone	6.0	6.0	0	14.5	0
No. 8 coal seam	5.5	5.5	0	13.5	0
Medium-grained sandstone	8.5	8.5	1.5	20.2	0
Argillaceous sandstone	7.5	7.5	1.0	19.5	0
Mudstone	6.0	6.0	0	14.5	0
No. 13 coal seam	5.5	5.5	0	13.5	0
Sandstone	8.5	8.5	1.5	20.2	0

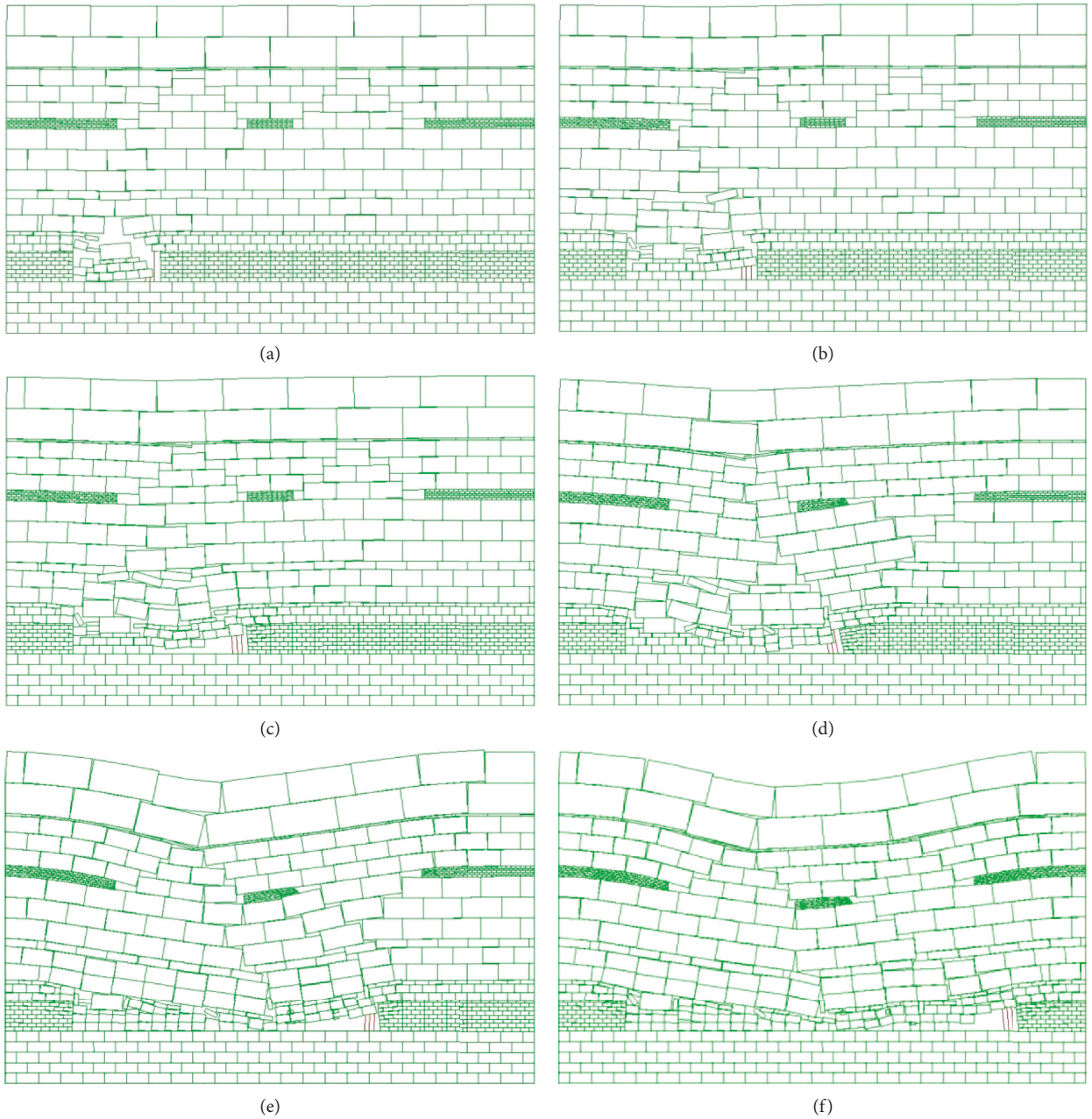

Figure 4: The evolution diagram of collapsing characteristics of overburden rock in the 60 m interlayer. Advance of the working face: (a) 40 m, (b) 60 m, (c) 80 m, (d) 100 m, (e) 140 m, and (f) 180 m.

20 m, and break through the upper goaf (Figure 5(a)). When the working face is advanced by 60 m, the total damage height reaches 30 m, there is no fracture or collapse of the main roof, and the interbedded strata push down with the working face (Figure 5(b)). When the working face advances 80 m, the overlying strata of the coal pillar break (Figure 5(c)). When the working face advances 100 m, it enters the coal pillar of the goaf. The immediate roof collapses, and the total damage height reaches 120 m (Figure 5(d)). When the working face advances 140 m, it enters the goaf, the interbedded strata collapse with the working face, and the total failure height reaches the upper boundary of the model (Figure 5(e)). When the working face advances 180 m, the overburden completely collapses and it forms a large "arch structures," and the support is in a "given load" state (Figure 5(f)). When the interlayer rock thickness is 15 m, it can be observed that the interlayer rock layer and the overlying rock layer gradually evolve into a large "arch structure" with a small "arch structure" as the working face advances, and the interlayer rock layer is an articulated block structure.

4. Discussion

4.1. Arch Structure and Its Stability of Interbedded Strata. When the interbedded strata are thick, the interbedded strata fall structure can be regarded as an "arch structure," as shown in Figure 6. Since the interlayer rock is not uniformly distributed by the pressure of the overlying rock formation, the interlayer rock formation eventually forms a loose layer arch structure in order to resist the uneven pressure. The overburden pressure will be transmitted from the vault to the arch that is still fixed in the stable rock formation, eventually forming a relatively stable space to protect the working face. When the loose layer arch structure advances to a certain distance on the working face, it will penetrate with the goaf of the old arch structure of the upper layer, which is characterized by the full thickness of the interlayer rock.

The working resistance of the support F_z consists of two parts, the gravity of main roof W and load from loose layer F_s.

The gravity of the main roof:

$$W = L_1 L_2 \rho_1 g h_1, \tag{1}$$

where L_1 is the control top distance of the support (m), L_2 is the width of the support (m), ρ_1 is the density of the main roof (kg/m^3), and h_1 is the thickness of the main roof (m).

Load from the loose layer:

$$F_s = \frac{d^2 \rho_2 g h_2}{3f}, \tag{2}$$

where d is the span of the arch (m), h_2 is the height of the free space in the stope (m), ρ_2 is the density of the loose layer (kg/m^3), and f is the solid constant of the loose layer.

Therefore, the working resistance of the bracket is as follows:

$$F_z = W + F_s = L_1 L_2 \rho_1 g h_1 + \frac{d^2 \rho_2 g h_2}{3f}. \tag{3}$$

4.2. Mass Block Structure and Its Stability of Interbedded Strata. When the interbedded strata are thinner, the interlayer rock layer is simplified to the block structure mechanical model, as shown in Figure 7. It is assumed that block No. 2 is in equilibrium, and the surrounding rock near the top plate is subjected to the combined force of the horizontal load and the combined force of the vertical load. If the interlayer rock mass is balanced only by its own weight and vertical stress, the following equations are obtained:

$$\begin{cases} N_3 = (W + Y_5)\cos\ \alpha, \\ T_3 = N_3 \tan\ \varphi_l, \\ T_3 = (W + Y_5)\sin\ \alpha, \end{cases} \tag{4}$$

where φ_l is the internal friction angle of the structural surface (°), α is the dip angle of fracture surface (°), W is the gravity of No. 2 rock sample (N), and Y_5 is the join force of No. 2 rock sample in the direction of q_y (N).

It can be obtained from the above equations, when $\alpha \le \varphi_l$, the No. 2 rock will be at rest; when $\alpha > \varphi_l$, the No. 2 rock will slide.

Based on the block equilibrium equation,

$$\begin{aligned} &(0, Y_5 + W) + N_3(\sin\ \alpha, -\cos\ \alpha) + N_4(-\sin\ \alpha,\ \cos\ \alpha) \\ &-\left[(N_3 + N_4)\tan\ \varphi_l + F_3 + F_4\right](\cos\ \alpha,\ \sin\ \alpha) = 0. \end{aligned} \tag{5}$$

From the left side of the No. 2 rock, it can be seen

$$\begin{cases} -T_3 \cos\ \alpha + N_3 \sin\ \alpha = X_3, \\ T_3 = N_3 \tan\ \varphi_l. \end{cases} \tag{6}$$

Namely, the equations can be transferred as follows:

$$\begin{cases} N_3 = \dfrac{X_3 \cos\ \varphi_l}{\sin(\alpha - \varphi_l)}, \\ T_3 = \dfrac{X_3 \sin\ \varphi_l}{\sin(\alpha - \varphi_l)}. \end{cases} \tag{7}$$

From the right side of the No. 2 rock, it can be seen

$$\begin{cases} -T_4 \cos\ \alpha - N_4 \sin\ \alpha = -X_4, \\ T_4 = N_4 \tan\ \varphi_l. \end{cases} \tag{8}$$

Also, the above equations can be transferred as follows:

$$\begin{cases} N_4 = \dfrac{X_4 \cos\ \varphi_l}{\sin(\alpha + \varphi_l)}, \\ T_4 = \dfrac{X_4 \sin\ \varphi_l}{\sin(\alpha + \varphi_l)}. \end{cases} \tag{9}$$

Therefore, the sliding force can be achieved as follows:

$$F = (Y_5 + W)\sin\ \alpha - \frac{X_3 \sin\ \varphi_l}{\sin(\alpha - \varphi_l)} - \frac{X_4 \sin\ \varphi_l}{\sin(\alpha + \varphi_l)}. \tag{10}$$

Since it is generated by the vertical load, the No. 2 rock is in equilibrium in the horizontal direction, so it is available:

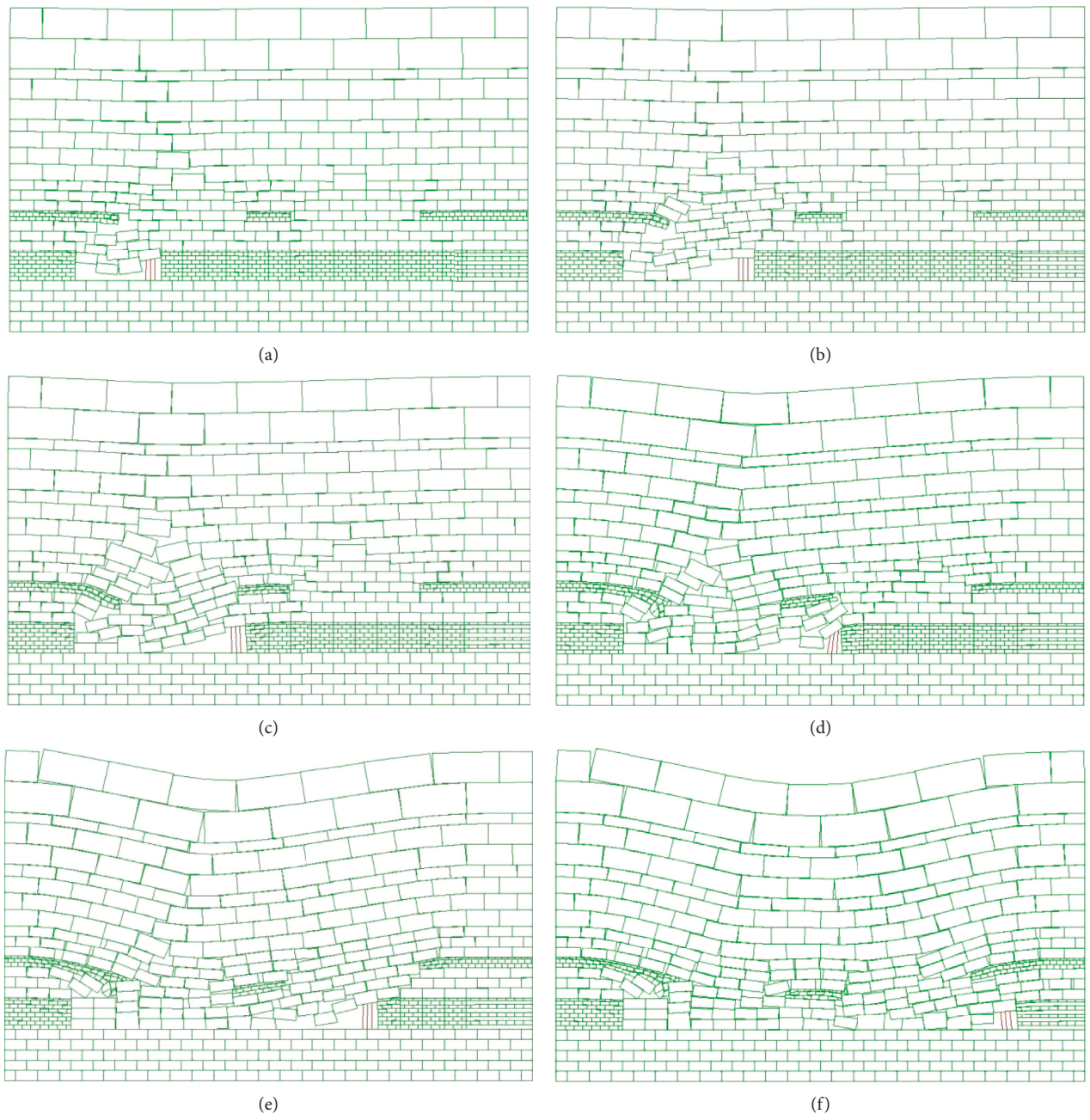

Figure 5: The evolution diagram of collapsing characteristics of overburden rock in the 15 m interlayer. Advance of the working face: (a) 40 m, (b) 60 m, (c) 80 m, (d) 100 m, (e) 140 m, and (f) 180 m.

Since Y_5 is generated by the vertical load q_y, that is, $Y = Y_5 = f(q_y)$, and X_3 and X_4 can be made by horizontal force q_x, the No. 2 rock mass is in equilibrium in the horizontal direction:

$$X = X_3 = X_4 = f(q_x). \tag{11}$$

Also, the sliding force F can be formulated as follows:

$$F = \left[f\left(q_y\right) + W\right]\sin\alpha - 2f(q_x)\frac{\cos\alpha\sin^2\alpha}{\sin(\alpha-\varphi_l)\sin(\alpha+\varphi_l)}. \tag{12}$$

The gravity of No. 2 rock W can be seen as follows:

$$W = \gamma V = \frac{\gamma IH}{\sin\alpha}, \tag{13}$$

where I is the width of cracks (m), H is the length of the block (m), and γ is the unit weight of the block (kg/m^3).

Then, the horizontal forces X and vertical forces Y can be shown as

$$\begin{cases} X = f(q_x) = q_x H, \\ Y = f\left(q_y\right) = q_y I. \end{cases} \tag{14}$$

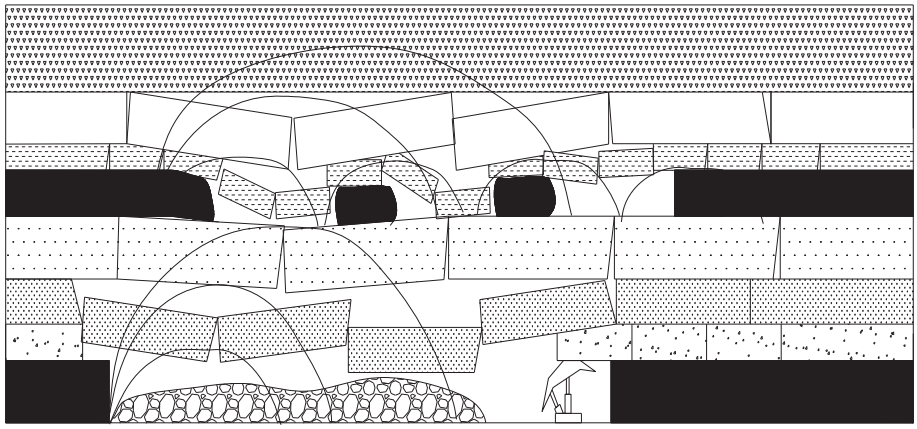

Figure 6: Mechanical model of the loose layer arch structure.

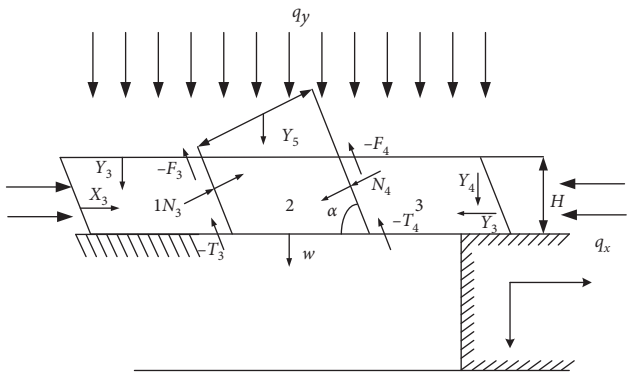

Figure 7: Computational model of the roof fracture.

Therefore, the sliding force F can be expressed as

$$F = q_y I \sin\alpha + \gamma H I \sin\alpha - 2q_x H \frac{\cos\alpha \sin^2\alpha}{\sin(\alpha-\varphi_l)\sin(\alpha+\varphi_l)}. \tag{15}$$

Assume $F > 0$ and $\alpha > \varphi_l$, the prevailing instability criterion can be shown:

$$\left(q_y + \gamma H\right) I \sin\alpha - 2q_x H \frac{\cos\alpha \sin^2\alpha}{\sin(\alpha-\varphi_l)\sin(\alpha+\varphi_l)} > 0. \tag{16}$$

4.3. Division of Three Zones. There is no uniform definition of close-distance coal seam mining, which is affected by the thickness of coal seam mining and overlying strata structure, interlayer rock stratum structure, and lithology. Along with the prevention and control of roof collapse and spontaneous combustion in extremely thick coal seam mining under the goaf, the adaptability to close and nonclose distances should also be considered. Liu [37, 38] calculated the empirical formulas of the height of the caving zone and the fracture zone as shown in Table 4, which was according to the lithology of the overlying strata. This method can be used generally to divide "three zones" of the depressing zones overlying a goaf, as the caving zone, fracture zone, and complete subsidence zone.

From the structural characteristics of the interlayer rock, whether the caving zone of lower coal seam is connected with the upper goaf as the boundary of the coal seam close-distance coal seam. When the mining thickness is 15 m, if the interlayer rock layers are all hard rock layers and less than 60 m or the interlayer rock layers are all soft stratum and less than 15 m, they are close-distance coal seams.

From the perspective of fire prevention and leakage prevention, whether the fracture zone of lower coal seams reaches the upper goaf as the boundary of the close-distance coal seam is identified. If the caving zone and the fracture zone are both hard rock layers and less than 100 m or both the caving zone and the fracture zone are soft rock layers and less than 35 m, they are close-distance coal seams.

(1) When the interlayer rock thickness is greater than 100 m, the interlayer rock layer gradually evolves into a large "arch structure" in the form of a small "arch structure" with the advancement of the working face, and "three zones" formed behind the working face in the interbedded strata, as shown in Figure 8. However, due to the thick interbedded strata, the maximum height of the "arch structure" is smaller than the thickness of the interlayer rock. Therefore, the presence of the upper goaf does not affect the "three zones" in the interbedded strata.

(2) When the thickness of the interlayer rock is less than 60 m, the lower goaf breaks in the form of block structure with the advancement of the working face and quickly penetrates with the upper goaf, and the entire overburden falls in the form of "arch structure," as shown in Figure 9. At this time, the fall zone of the upper goaf is affected by the secondary disturbance, the fracture zone becomes a new caving zone, and the complete subsidence zone becomes a new fracture zone.

(3) When the thickness of the interlayer rock is between 60 and 100 m, the interbedded strata will gradually evolve into a large "arch structure" in the early stage of the working face advancement, and the upper goaf will not affect the "three zones" in the interlayer rock layer. When the height of the "arch structure"

Table 4: Traditional empirical calculation formula of collapsed and fractured zone height.

Lithology	Maximum height of caving zone (m)	Maximum height of fracture zone (m)
Hard rock	$H_k = ((100\sum M)/(2.1\sum M + 16)) \pm 2.5$	$H_d = ((100\sum M)/(1.2\sum M + 2.0)) \pm 8.9$
Medium-hard rock	$H_k = ((100\sum M)/(4.7\sum M + 19)) \pm 2.2$	$H_d = ((100\sum M)/(1.6\sum M + 3.6)) \pm 5.6$
Soft stratum	$H_k = ((100\sum M)/(6.2\sum M + 32)) \pm 1.5$	$H_d = ((100\sum M)/(3.1\sum M + 5.0)) \pm 4.0$
Extremely weak rock	$H_k = ((100\sum M)/(7.0\sum M + 63)) \pm 1.2$	$H_d = ((100\sum M)/(5.0\sum M + 8.0)) \pm 3.0$

M: thickness of the coal seam; ± is the margin of error.

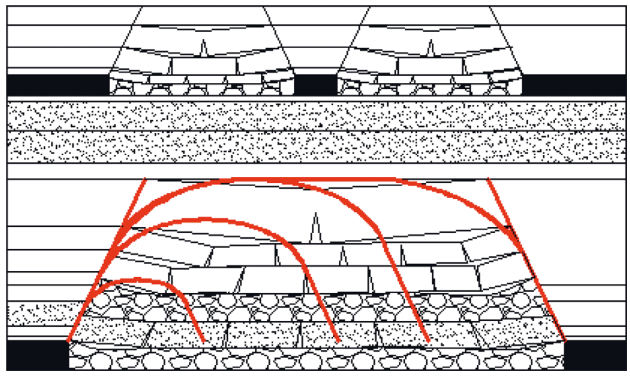

Figure 8: The relationship between upper gob and lower gob under the condition of thick layer strata.

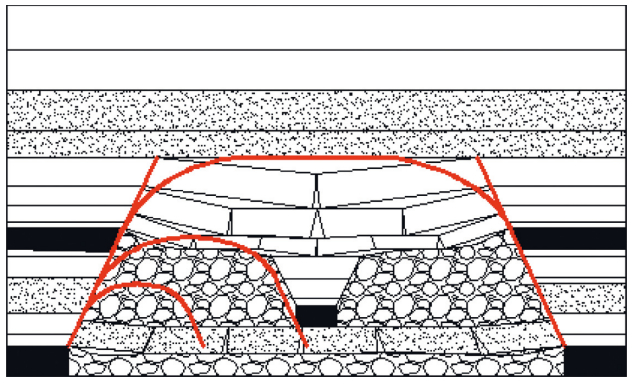

Figure 9: The relationship between upper goaf and lower goaf under the condition of thin layer strata.

reaches the thickness of the interbedded strata and continues to develop upwards, it will penetrate with the upper goaf. At this time, the upper goaf will cave. The zones are subjected to secondary disturbances, the old fracture zone becomes a new caving zone, and the complete subsidence zone becomes a new fracture zone.

5. Conclusions

According the physical simulation, numerical simulation, and theoretical analysis, the different thickness interbedded strata and their collapse during the mining of extremely thick coal seam were studied. The main conclusions can be drawn as follows:

(1) From the structural characteristics of the interbedded strata, whether the caving zone of the lower coal seam is connected with the upper goaf as the boundary of the coal seam close-distance coal seam is identified; from the perspective of fire prevention and leakage prevention, whether the fracture zone of lower coal seam is connected with the upper goaf as the boundary of the close-distance coal seam is identified

(2) When the interbedded strata is thin, the interlayer rock falls in the form of block structure caving, overlying strata are "arch structure" in the form of caving; when the interbedded strata is thick, the interlayer rocks are in the form of "arch structure"

(3) When the interbedded strata are thinner, the first top coal caving, the first immediate roof caving, the first roof weighting, and the maximum working resistance of the hydraulic support are relatively earlier than thick interlayer, while the periodic roof weighting pace and the angle of the top coal and immediate roof have no significant changes

(4) The maximum working resistance of the hydraulic support under different conditions occurs when the working face enters and exits the pillar of coal

Data Availability

The article data used to support the findings of this study are included within the article.

Conflicts of Interest

The authors declare that there are no conflicts of interest regarding the publication of this paper.

Acknowledgments

This work was supported by the State Key Laboratory for Geo-Mechanics and Deep Underground Engineering (Grant no. SKLGDUEK1410), State Key Laboratory of Coal Resources and Safe Mining (Grant no. SKLCRSM14KFB08), Key Research and Development Project of Shanxi Province (201803D31051), Open Project of Research Center of Coal Resources Safe Mining and Clean Utilization, Liaoning (Grant no. LNTU17KF07), National Natural Science Foundation of China (Grant no. 51404167), China Postdoctoral Science Foundation funding project (Grant no. 2016M590151), and Scientific and Technologial Innovation Programs of Higher Education Institutions in Shanxi (Grant no. STIP 201802047).

References

[1] Y. K. Yang, T. H. Kang, Y. Lan et al., "Study of mining method of L-shaped Working face by full-mechanized sublevel caving mining shallow-buried thick coal seam and its underground pressure field observation," *Chinese Journal of Rock Mechanics and Engineering*, vol. 2, pp. 244–253, 2011.

[2] P. Huang, F. Ju, K. Jessu, M. Xiao, and S. Guo, "Optimization and practice of support working resistance in fully-mechanized top coal caving in shallow thick seam," *Energies*, vol. 10, no. 9, p. 1406, 2017.

[3] Y. K. Yang, *Research on Overlying Strata Movement Law and Surrounding Rock Control of Full-Seam Mining for Extremely Thick Coal Seam by Sub-Level Caving Mining with High Bottom Cutting Height*, Coal Industry Press, Beijing, China, 4th edition, 2014.

[4] J. Wang, B. Yu, H. Kang et al., "Key technologies and equipment for a fully mechanized top-coal caving operation with a large mining height at ultra-thick coal seams," *International Journal of Coal Science and Technology*, vol. 2, no. 2, pp. 97–161, 2015.

[5] R. Singh, "Staggered development of a thick coal seam for full height working in a single lift by the blasting gallery method," *International Journal of Rock Mechanics and Mining Sciences*, vol. 41, no. 5, pp. 745–759, 2004.

[6] S. S. Peng, *Coal Mine Ground Control*, Wiley, New York, NY, USA, 2nd edition, 1986.

[7] H. Alehossein and B. A. Poulsen, "Stress analysis of longwall top coal caving," *International Journal of Rock Mechanics and Mining Sciences*, vol. 47, no. 1, pp. 30–41, 2010.

[8] A. M. Suchowerska, R. S. Merifield, and J. P. Carter, "Vertical stress changes in multi-seam mining under supercritical longwall panels," *International Journal of Rock Mechanics and Mining Sciences*, vol. 61, pp. 306–320, 2013.

[9] F. Gao, D. Stead, and J. Coggan, "Evaluation of coal longwall caving characteristics using an innovative UDEC Trigon approach," *Computers and Geotechnics*, vol. 55, pp. 448–460, 2014.

[10] J. Ning, J. Wang, L. Jiang, N. Jiang, X. Liu, and J. Jiang, "Fracture analysis of double-layer hard and thick roof and the controlling effect on strata behavior: a case study," *Engineering Failure Analysis*, vol. 81, pp. 117–134, 2017.

[11] Y. Liu, F. Zhou, L. Liu, C. Liu, and S. Y. Hu, "An experimental and numerical investigation on the deformation of overlying coal seams above double-seam extraction for controlling coal mine methane emissions," *International Journal of Coal Geology*, vol. 87, no. 2, pp. 139–149, 2011.

[12] G. Cheng, C. Chen, L. Li et al., "Numerical modelling of strata movement at footwall induced by underground mining," *International Journal of Rock Mechanics and Mining Sciences*, vol. 108, pp. 142–156, 2018.

[13] S. Gu, B. Jiang, G. Wang, H. Dai, and M. Zhang, "Occurrence mechanism of roof-fall accidents in large-section coal seam roadways and related support design for bayangaole coal mine, China," *Advances in Civil Engineering*, vol. 2018, Article ID 6831731, 17 pages, 2018.

[14] G. C. Yan, *Research on Theory and Technology of Joint Mining of Short Distance Coal Seam Group*, Taiyuan University of Technology, Taiyuan, China, 2009.

[15] Z. Zhu, T. Feng, Z. Yuan, D. Xie, and W. Chen, "Solid-gas coupling model for coal-rock mass deformation and pressure relief gas flow in protection layer mining," *Advances in Civil Engineering*, vol. 2018, Article ID 5162628, 6 pages, 2018.

[16] D. Zhang, G. Fan, L. Ma, and X. Wang, "Aquifer protection during longwall mining of shallow coal seams: a case study in the Shendong Coalfield of China," *International Journal of Coal Geology*, vol. 86, no. 2-3, pp. 190–196, 2011.

[17] X. Lai, M. Cai, F. Ren, M. Xie, and T. Esaki, "Assessment of rock mass characteristics and the excavation disturbed zone in the Lingxin Coal Mine beneath the Xitian river, China," *International Journal of Rock Mechanics and Mining Sciences*, vol. 43, pp. 572–581, 2006.

[18] T. Zhu, B. S. Zhang, and G. R. Feng, "Roof structure and control of coal seam under coal seam under very close distance," *Journal of China Coal Society*, vol. 35, pp. 190–193, 2010.

[19] W. B. Zhu, J. L. Xu, and X. S. Shi, "Research on influence of overburden primary key stratum movement on surface subsidence with in-situ drilling test," *Chinese Journal of Rock Mechanics and Engineering*, vol. 28, no. 2, pp. 403–409, 2009.

[20] G. L. Guo, X. X. Miao, and Z. N. Zhang, "Research on ruptured rock mass deformation characteristics of longwall goafs," *Science Technology and Engineering*, vol. 2, pp. 44–47, 2002.

[21] C. C. He and J. L. Xu, "Subsidence prediction of overburden strata and surface based on the voussoir beam structure theory," *Advances in Civil Engineering*, vol. 2018, Article ID 2606108, 13 pages, 2018.

[22] Z. J. Wen, R. Mikael, and Z. Song, "Research on modelling of spatial dynamic structural mechanics and spatio-temporal evolution of coal mine stopes," *Tehnicki Vjesnik-Technical Gazette*, vol. 22, no. 3, pp. 607–613, 2015.

[23] Z. Wen, Y. Tan, Z. Han, and F. Meng, "Construction of time-space structure model of deep stope and stability analysis," *Polish Journal of Environmental Studies*, vol. 25, no. 6, pp. 2633–2639, 2016.

[24] C. Wang, T. Bao, H. Lu et al., "Variation regulation of the acoustic emission energy parameter during the failure process of granite under uniaxial compression," *Materials Testing*, vol. 57, no. 9, pp. 755–760, 2015.

[25] D. K. Wang, J. P. Wei, and Z. H. Wen, "Permeability characteristics of gas-bearing coal under different stress paths," *Disaster Advances*, vol. 6, pp. 289–294, 2013.

[26] D. K. Wang, S. M. Liu, J. P. Wei, H. L. Wang, and B. H. Yao, "A research study of the intra-nanopore methane flow law," *International Journal of Hydrogen Energy*, vol. 42, no. 29, pp. 18607–18613, 2017.

[27] S. Feng, S. Sun, Y. Lv, and J. Lv, "Research on the height of water flowing fractured zone of fully mechanized caving mining in extra-thick coal seam," *Procedia Engineering*, vol. 26, pp. 466–471, 2011.

[28] B. Yu, J. Zhao, T. Kuang, and X. Meng, "In situ investigations into overburden failures of a super-thick coal seam for longwall top coal caving," *International Journal of Rock Mechanics and Mining Sciences*, vol. 78, pp. 155–162, 2015.

[29] C. L. Wang, G. Y. Li, and A. S. Gao, "Optimal pre-conditioning and support designs of floor heave in deep roadways," *Geomechanics and Engineering*, vol. 14, pp. 429–437, 2018.

[30] Q. X. Huang, *Study on Roof Structure and Rock Stratum Control of Longwall Mining in Shallow Coal Seam*, China University of Mining and Technology Press, Xuzhou, China, 2000.

[31] J. L. Xu, D. Cai, and K. L. Fu, "Mechanism of supports crushing accident and its preventive measures during coal mining near unconsolidated confined aquifer," *Journal of China Coal Society*, vol. 32, pp. 1239–1243, 2017.

[32] J. Ju and J. Xu, "Structural characteristics of key strata and strata behaviour of a fully mechanized longwall face with 7.0m height chocks," *International Journal of Rock Mechanics and Mining Sciences*, vol. 58, pp. 46–54, 2013.

[33] I. A. Wright, B. McCarthy, N. Belmer, and P. Price, "Subsidence from an underground coal mine and mine wastewater discharge causing water pollution and degradation of aquatic ecosystems," *Water, Air, and Soil Pollution*, vol. 226, no. 10, p. 348, 2015.

[34] L. Q. Ma, D. S. Zhang, and G. J. Sun, "Thick alluvium full-mechanized caving mining with large mining height face roof control mechanism and practice," *Journal of China Coal Society*, vol. 38, no. 2, pp. 199–203, 2013.

[35] V. Palchik, "Formation of fractured zones in overburden due to longwall mining," *Environmental Geology*, vol. 44, no. 1, pp. 28–38, 2003.

[36] Z. Hu, F. Hu, J. Li, and H. Li, "Impact of coal mining subsidence on farmland in eastern China," *International Journal of Surface Mining, Reclamation and Environment*, vol. 11, no. 2, pp. 91–94, 1997.

[37] T. Q. Liu, "Mining rock mass mining influence and control engineering and its application," *Journal of China Coal Society*, vol. 20, no. 1, pp. 1–5, 1995.

[38] E. F. Salmi, M. Nazem, and M. Karakus, "Numerical analysis of a large landslide induced by coal mining subsidence," *Engineering Geology*, vol. 217, pp. 141–152, 2017.